Tight-binding studies of uniaxial strain in T-graphene nanoribbons

OPEN ACCESS
IOP Publishing
Journal of Physics: Condensed Matter
J. Phys.: Condens. Matter **34** (2022) 214001 (8pp)
https://doi.org/10.1088/1361-648X/ac5a02

Tight-binding studies of uniaxial strain in T-graphene nanoribbons

J Hopkinson[1] **and Y Hancock**[1,2,*]

[1] Department of Physics, University of York, Heslington, York YO10 5DD, United Kingdom
[2] York Cross-disciplinary Centre for Systems Analysis, University of York, Heslington, York YO10 5GE, United Kingdom

E-mail: y.hancock@york.ac.uk

Received 8 November 2021, revised 17 February 2022
Accepted for publication 2 March 2022
Published 21 March 2022

Abstract

The role of uniaxial strain in armchair, T-graphene nanoribbons (ATGNRs) with symmetric and asymmetric structures is investigated using a nearest-neighbour, tight-binding (TB) model. ATGNRs with structural symmetry and two a sub-lattice structure exhibit Dirac points at zero strain. Application of uniaxial strain to these systems induces multiple Dirac points under compression (up to −20% strain), with the number of these points commensurate with the number of tetra-carbon base-units along the width of the unit cell, accounting also for the mirror symmetry of the structure. Under tensile, uniaxial strain (up to 20% extension), the induced asymmetry in the carbon tetrabond results in the number of Dirac points being reduced, although a minimum number are preserved due to the fundamental mirror-symmetry of the symmetric ATGNR. Asymmetric ATGNRs, which are semiconductors, are shown to have tunable band-gaps that decrease as a function of increasing ribbon width and uniaxial strain. Uniaxial strain induces a single Dirac point at the band edge of these systems under high compression (>16%), with the closing of the band gap linked to symmetry-induced perturbations in the structure that override the symmetry-breaking, gap-opening mechanisms. In summary, the TB model shows ATGNRs to have suitable device features for flexible electronics applications, such as band-gap tuning, and for the strain engineering of relativistic properties.

Keywords: tight-binding studies, strain engineering, T-graphene nanoribbons, relativistic properties, Dirac systems

(Some figures may appear in colour only in the online journal)

* Author to whom any correspondence should be addressed.

1. Introduction

Graphene—a 2D allotrope of carbon—needs no introduction. Its remarkable properties on the bulk length scale (e.g., high charge-carrier mobility, strength and flexibility) have resulted in numerous studies and an intense drive to realise applications [1]. Most notable about this system are its relativistic properties that arise from the linear, electronic dispersion about the Fermi energy, these being the so-called Dirac cones [2, 3]. Although bulk graphene is without a natural band gap, one can be realised on the nanoscale, for example, in graphene nanoribbons (GNRs; nm-width strips of graphene) due to edge effects and quantum confinement. In both simulation and experiment, the band gaps of GNRs vary inversely as a function of increasing ribbon width [4, 5] and are also tunable as a function of strain [6], the latter being a property amenable to applications in flexible electronics.

The physical realisation of graphene has stimulated the field of 2D-materials research resulting in several new systems being proposed and fabricated, such as silicene and germanene (single layers of silicon and germanium) [7, 8], and monolayer transition-metal dichalcogenides [9]. See also references [10, 11], as well as articles therein for detailed reviews. Studies of the Dirac-cone features, specifically the low-energy, linear energy dispersion, which gives rise to the desired relativistic properties of graphene and these other 2D systems, have ensured. Such studies include experimental verification of the relativistic features, such as the prevalence of massless charge carriers with ultra-high mobilities [12], with up to 10^5 cm^2 V^{-1} s^{-1} charge-carrier mobility reported in suspended graphene [13]. Robustness testing of the Dirac-cone properties against structural deformation and patterning, and mechanisms for Dirac-cone formation and tunability, the latter pertaining to k-space displacement and relativistic on/off properties, have also been reported (e.g., [11, 14–16]).

A key feature attributed to the mechanism for Dirac-cone formation has been the intrinsic, underlying honeycomb lattice structure of these systems [11]. Thus, of particular interest are 2D-carbon systems that are without honeycomb-lattice symmetry, but have propensity to form Dirac cones. Examples include buckled T-graphene [17], S-graphene [18] and certain graphyne variants (e.g., reference [19]). T-graphene, a two-dimensional tetra-symmetric carbon allotrope, is of particular interest as it is predicted by density functional theory (DFT) to have high stability with a cohesive energy of −9.4 eV/atom versus −9.9 eV/atom for graphene [20]. In its buckled form, planar T-graphene exhibits two Dirac points with associated linear dispersion that persist for up to ∼20% strain [17], similar to strained graphene [14]. The modest out-of-plane buckling of the T-graphene structure between two nearest-neighbour carbon tetrarings (0.55 Å) is sufficient to induce a two sublattice structure and real-space symmetry with resulting π and π^* crossings—these being attributed to the formation mechanism of the Dirac points [17]. Underlying all of these linear dispersion-forming systems are protective symmetries of various origins [18, 21, 22].

In this paper, we investigate the electronic properties of armchair T-graphene nanoribbons (ATGNRs) under uniaxial strain within the tight-binding (TB) formalism. DFT studies show that ATGNRs with structural symmetry (figure 1(a)) have resultant low-energy, linear dispersion features (i.e., Dirac points), whereas structurally asymmetric systems (figure 1(b)) have semiconductor properties via symmetry-breaking mechanisms [17, 23]. These symmetry-induced properties pertaining to Dirac-point formation have been fundamentally characterised using TB [23]. In this work, we will extend this understanding to investigate the application of uniaxial strain within the TB formalism to determine (i) the robustness of the linear dispersion and Dirac points against structural modifications, and (ii) any symmetry-related mechanisms for strain-induced, Dirac-feature formation, particularly in asymmetrically-structured, semiconductor ATGNRs. The use of a minimal TB model will enable computationally-efficient calculations at ultra-fine sampling to investigate these features and the ability to probe underlying mechanisms that specifically relate to the kinetics of the model, such as strain-induced electronic confinement and structural symmetry changes, commensurate also with changes in the ribbon width. In addition to these investigations, we will also provide a comparison to the electronic properties of armchair graphene nanoribbons (AGNRs) (figure 1(c)) and, in general, also place this work into the broader context of study of structural and symmetry-related classes of low-dimensional Dirac systems. Such studies may add fundamental understanding of the role of symmetry in engineering relativistic features and stimulate greater research into ATGNRs as tunable electronic devices within the realm of flexible electronics.

2. Method

The ATGNRs and AGNRs are investigated using spin-independent, TB model,

$$\hat{H} = -\sum_{ij} t_{ij} c_i^\dagger c_j + \text{H.c.} \tag{1}$$

Here, $c_i^\dagger(c_j)$ is the fermion creation (destruction) operator that creates (destroys) an electron at site i (j) and H.c. denotes the Hermitian conjugate. The carbon atoms in these systems are considered to be chemically equivalent; hence, the on-site energies are set to zero. For the ATGNRs, the parameterisation in Dai *et al* (2014) is used with hopping integrals $t_{1a} = 2.525$ eV and $t_{1b} = 2.835$ eV for the nearest-neighbour $1a$ and $1b$ bonds, respectively (figures 1(a) and (b)). The AGNRs are modelled using the parameter set in Hancock *et al* (2010) [24] with up to third nearest-neighbour hopping ($t_1 = 2.7$ eV, $t_2 = 0.20$ eV and $t_3 = 0.18$ eV for first, second and third nearest-neighbour hopping, respectively), and with edge-perturbation to the hopping to capture hydrogen passivation ($t_{\text{edge}} = 1.06t_1$) (figure 1(c)). Band structures are determined from the numerical eigenenergy solutions of the Hamiltonian matrix generated from equation (1), which has been calculated along the one-dimensional, first Brillouin zone using k-point increments of 0.001 Å^{-1} in units of π/a, where a denotes the unit-cell dimension of each system.

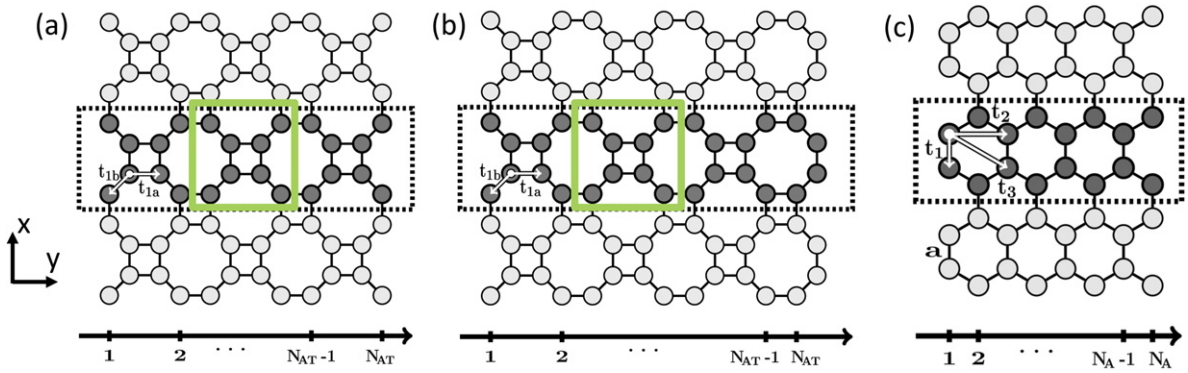

Figure 1. Unit cells (boxed) for (a) symmetric and (b) asymmetric ATGNRs, showing exemplar 6-ATGNR and 7-ATGNR systems, respectively, and for the (c) AGNR (8-AGNR). N_{AT} and N_A denote the naming conventions specific to the ribbon widths for N_{AT}-ATGNRs and N_A-AGNRs. t_{1a} and t_{1b} are the nearest-neighbour hopping parameters for ATGNRs, with AGNRs having up to third nearest-neighbour hopping (t_1, t_2 and t_3). The fundamental, tetra-based units for the ATGNRs are highlighted in green.

Uniaxial strain is implemented via Harrison scaling of the hopping parameters in equation (1) [25],

$$t'_{ij} = t_{ij}\left(\frac{r_0}{r}\right)^2, \tag{2}$$

where t_{ij} and t'_{ij} are the unstrained and strained hopping integrals between sites i and j, and r_0 and r are the unstrained and strained bond lengths, respectively. For a given strain,

$$\epsilon = \frac{r - r_0}{r_0}. \tag{3}$$

In this respect, we define ϵ_x as the uniaxial strain in the x-direction (along the ribbon length) and ϵ_y as the uniaxial strain in the y-direction (along the ribbon width), such that

$$\epsilon_y = -P\epsilon_x. \tag{4}$$

Here, $P = 0.24$ is the Poisson ratio derived from DFT calculations on bulk T-graphene [6], which we have used as an approximate value for the ATGNRs.

3. Results and discussion

The TB model with nearest-neighbour hopping reproduces with good approximation, the low-energy, band structure features of ATGNRs against published DFT results [23] for both the symmetric (figures 2(a)–(d)) and asymmetric (figures 2(e)–(h)) cases. The unit cell for symmetric ATGNRs has as its base unit, a fundamental, two sub-lattice structure, and mirror symmetry (figure 1(a)) akin to buckled, planar T-graphene, which translates to Dirac points in k-space (figures 2(a)–(d)). In asymmetric ATGNRs, the structural symmetry of the unit cell is broken (figure 1(b)), thereby inducing a gap-opening mechanism at the Fermi-level [23], which is captured also in the TB results (figures 2(e)–(h)). For both systems, the number of nodal points across k-space increases for increasing unit-cell size (system width) in concordance with the number of structural base-units.

Nearest-neighbour hopping in ATGNRs is sufficient to capture the essential features of the gap versus width trends as shown in the TB and DFT comparisons (figure 3(a)). Asymmetric (odd) ATGNRs are semiconductors with a band gap that varies inversely as a function of increasing ribbon width, similar to AGNRs (cf figure 3(b)). However, structurally-symmetric ATGNRs remain gapless due to the two sublattice structure and mirror, structural symmetry. Symmetric ATGNRs can be compared to 3p + 2 AGNRs, which are also structurally symmetric and zero-gapped in the nearest-neighbour TB model, but, in contrast to symmetric ATGNRs, have a finite gap in the DFT that is reproduced by adding edge-perturbation and third nearest-neighbour hopping to the TB simulation [5, 26].

The TB results in figure 3 are fitted using $E_{gap} = A\,e^{-\lambda w} + c$ as the best choice of function over this fitting range. The exponential fitting shows asymmetric ATGNRs have a rate of decrease in gap ($-\lambda$) versus width (w) equivalent to the AGNR 3p and 3p + 1 families ($\lambda = 0.15$), although AGNR band gaps remain relatively higher at ∼60% mean difference compared to ATGNRs across this range of widths. Within the TB simulation, asymmetric ATGNRs approach room-temperature thermal viability with band gaps $> k_B T = 0.03$ eV at 300 K for widths less than 30 Å, as opposed to AGNRs, which remain thermally viable for all of the widths reported here.

Uniaxial strain (ϵ_x) is applied to the x-direction of the ATGNRs (i.e., along the ribbon length) with upper and lower values at ±0.2 commensurate with limits determined by DFT and molecular dynamics studies of T-graphene nanosystems (e.g., fracture strains reported between 0.17–0.24 [27–29]). For the 2-ATGNR, the TB model shows the Dirac point and its associated linear dispersion to be conserved up to the extreme values of strain ($\epsilon_x = \pm 0.2$), albeit with displacement in k-space as a function of the induced structural perturbation (figure 4).

Corresponding bond length modifications and Dirac point features for the 2-ATGNR, including the linear dispersion range obtained upon fitting versus the applied uniaxial strain at $\epsilon_x = 0$ and ±0.2, are shown in table 1. In accordance with equations (2)–(4), a negative, compressive strain increases hopping (decreases bond length) in the x-direction, and decreases hopping (increases bond length) in the y-direction,

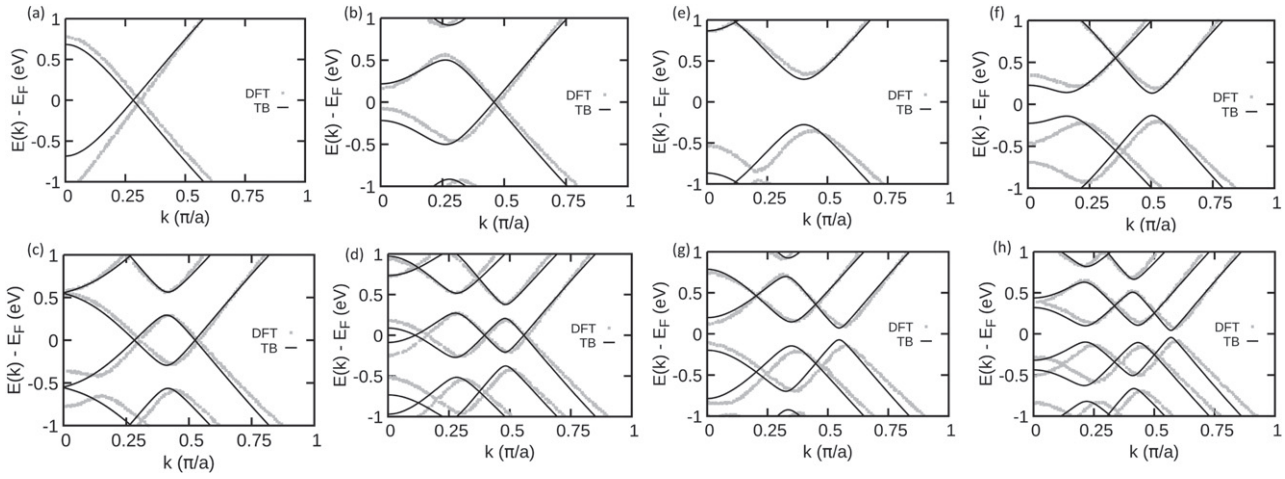

Figure 2. Band structures centred at the Fermi energy (E_F) as a function of ribbon width for the structurally-symmetric (a) 2-ATGNR, (b) 4-ATGNR, (c) 6-ATGNR and (d) 8-ATGNR, and structurally-asymmetric (e) 3-ATGNR, (f) 5-ATGNR, (g) 7-ATGNR and (h) 9-ATGNR systems (cf figures 1(a) and (b), respectively). The plots show favourable comparison of the TB model (this work; black lines) against the DFT results extracted from Dai *et al* (figure 2, reference [23]; grey lines). Here, '*a*' denotes the unit-cell dimension for each system.

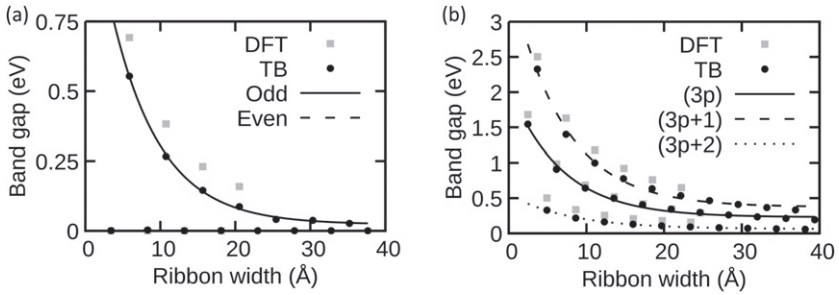

Figure 3. Band gap versus increasing ribbon width for (a) ATGNRs calculated using the TB model with nearest-neighbour hopping (cf figure 1(a)) versus the DFT results of Dai *et al* (2014) (figure 2 in reference [23]), and for (b) AGNRs calculated using an extended TB model with up to third nearest-neighbour hopping and edge-perturbation versus the DFT results from reference [24]. Asymmetric (odd) ATGNRs are semiconductors (i.e., have finite gaps), whereas symmetric (even) ATGNRs are gapless. All cases show good comparisons between TB and DFT.

with the opposite being true for positive, tensile strain. The perturbed bond lengths within the TB model at $\epsilon_x = 0.2$ (i.e., 1.398 Å, 1.498 Å and 1.762 Å) are within the approximate range for those obtained by DFT for T-graphene, e.g., 1.65 Å maximum bond length at an upper limit of 0.24 strain [27], and from molecular dynamics simulations, e.g., 1.3–1.8 Å bond-lengths obtained from 0 to 0.25 strain, and 1.32 Å, 1.45 Å and 1.72 Å bond lengths at 0.17 strain (see figure S1, reference [29]). For the compressive case ($\epsilon_x = -0.2$), the bond lengths, 1.289 Å and 1.538 Å, are also comparable to the aforementioned values, whereas the bond length of 1.174 Å approximates that of a carbon triple bond.

To understand the mechanism for the displacement of the Dirac point as a function of uniaxial strain, a symbolic, analytical solution for the energy eigenvalues corresponding to the 8 × 8 Hamiltonian matrix for the 2-ATGNR was obtained using Mathematica. Setting $E = 0$, a doubly-degenerate, lowest-energy solution was found, with the expression for the Dirac k-point as a function of the applied uniaxial strain (ϵ_x) determined as

$$k_{\mathrm{D}}(\epsilon_x) = \cos^{-1}\left(\frac{t_{ax}^2(\epsilon_x)}{2t_b^2(\epsilon_x)} + \frac{t_b^2(\epsilon_x)}{2t_{ax}^2(\epsilon_x)} - \frac{t_{ay}^2(\epsilon_x)}{2t_b^2(\epsilon_x)}\right), \quad (5)$$

where

$$t(\epsilon_x) = \frac{t_0}{(\epsilon_x + 1)^2\cos^2\theta + (-P\epsilon_x + 1)^2\sin^2\theta} \quad (6)$$

is the general expression for the hopping as a function of strain. Here, $t(\epsilon_x) = t_{ax}(\epsilon_x)$ at $\theta = 0°$, $t_{ay}(\epsilon_x)$ at $\theta = 90°$ and $t_b(\epsilon_x)$ at $\theta = 45°$, where θ is the angle relative to the vertical tetrahedral bond in the x-direction (along the ribbon width), t_0 is the initial hopping value for the bond at $\epsilon_x = 0$, and $P = 0.24$ is the Poisson ratio for T-graphene (see also equations (2) and (4)).

When the tetrahedral bond lengths are equal at zero applied strain ($\epsilon_x = 0$), then $t_{ax} = t_{ay} = t_a$ and equation (5) reduces to $k_{\mathrm{D}}(\epsilon_x) = \cos^{-1}\left(\frac{t_b^2}{2t_a^2}\right)$. For compressive strain in the x-direction, i.e., negative strain values, then $t_{ax} > t_{ay}$ creates an asymmetry in the argument of equation (5) that shifts the Dirac k-point to the left, and vice versa for the case of positive strain

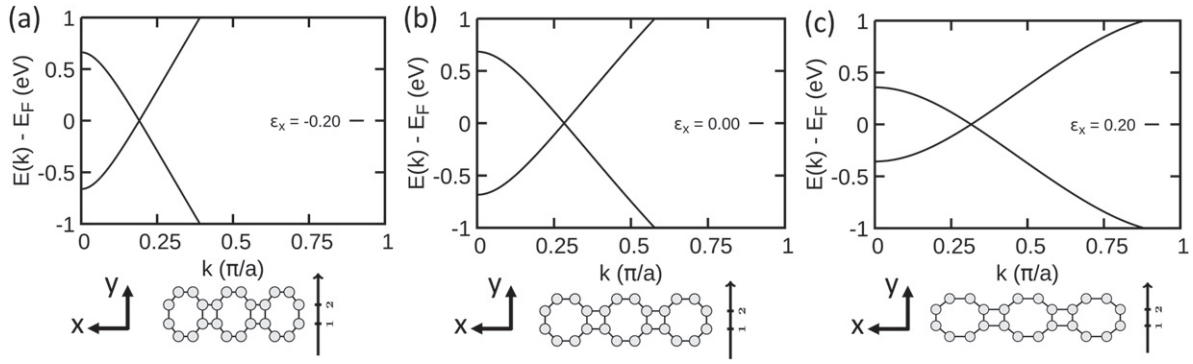

Figure 4. Band structures for the 2-ATGNR with (a) −0.2, (b) zero and (c) 0.2 uniaxial strain (ϵ_x) applied along the ribbon length, and corresponding representative structures that show the resultant structural perturbations. Here, 'a' is the unit cell dimension for each system. The displacement of the Dirac point in k-space as a function of the applied strain corresponds to asymmetric changes in the real-space unit cell due to strain perturbation.

Table 1. 2-ATGNR with applied uniaxial strain (ϵ_x) along the ribbon length showing the perturbation to the bond lengths, TB parameters and features corresponding to the Dirac points (positions and linear-dispersion ranges).

Strain ϵ_x	−0.2	0	0.2
Horiz. tetrabond (Å)	1.538	1.468	1.398
t_{ay} horizontal (eV)	[2.299]	[2.525]	[2.786]
Vert. tetrabond (Å)	1.174	1.468	1.762
t_{ax} vertical (eV)	[3.945]	[2.525]	[1.753]
Inter. tetrabond (diag.) (Å)	1.289	1.383	1.498
t_b diagonal (eV)	[3.260]	[2.835]	[2.412]
Dirac point features (numerically determined)			
k-point position (π/a)	0.19	0.28	0.32
Linear-dispersion range (±eV)	0.16	0.10	0.05

extension, with these results making transparent the underlying, symmetry-breaking mechanism associated with the Dirac point shift, and confirming the numerical findings in figure 4 and table 1.

The number of Dirac points for symmetric ATGNRs evolve as a function of increasing ribbon width and strain as illustrated by the 6-ATGNR band structures in figure 5. Compressive strain at $\epsilon_x = -0.2$ leads to longer bond lengths and reduced hopping in the y-direction (t_{ay}), such that the system is effectively reduced to multiple, weakly-coupled 2-ATGNR chains (figure 5(d)). In the case of the 6-ATGNR, there are three 2-ATGNR chains with tetra-based sub-units as shown in figure 1(a), which translate to the same number of Dirac points in k-space (figure 5(a)). For the zero-strain result, the mirror-plane and tetra carbon-ring symmetries ($t_{ax} = t_{ay}$) in the two sub-systems for the 6-ATGNR lead to two Dirac points (figures 5(b) and (e); see also [23]), whereas in the tensile strain (positive strain) case, asymmetry in the tetra sub-unit ($t_{ax} < t_{ay}$), yet preservation of the structural mirror-symmetry, results in a single Dirac point (figures 5(c) and (f)). The TB prediction, therefore, not only demonstrates the robustness of the Dirac points in symmetric ATGNRs under uniaxial strain, but also the tunability of the number of these points by strain engineering linked to changes in structural symmetry and quantum confinement.

Asymmetric ATGNRs are semiconductors due to their structural asymmetry (figure 2(b)). Upon application of uniaxial strain (ϵ_x), the band gap increases for these systems with positive, tensile strain and decreases for negative, compressive strain irrespective of the system size (figures 6(a)–(d) for 3-, 5-, 7- and 9-ATGNRs, respectively). This finding is commensurate with the change in energetics of the system; a lengthening of bonds in the x-direction under tensile strain results in greater quantum confinement along the ribbon width and a reduction of the kinetics, i.e., reduced value of the hopping, t_{ax} (cf equation (2)) in the direction of periodicity. The increased quantum confinement against the direction of periodicity causes further gap opening, whereas the converse is true under compression. Similarly, greater quantum confinement along the ribbon width for smaller-width systems results in larger band gaps against larger-width systems at the same values of comparative strain. The gap versus strain results as a function of system size shows points where the band gap closes, with the number of these points increasing as a

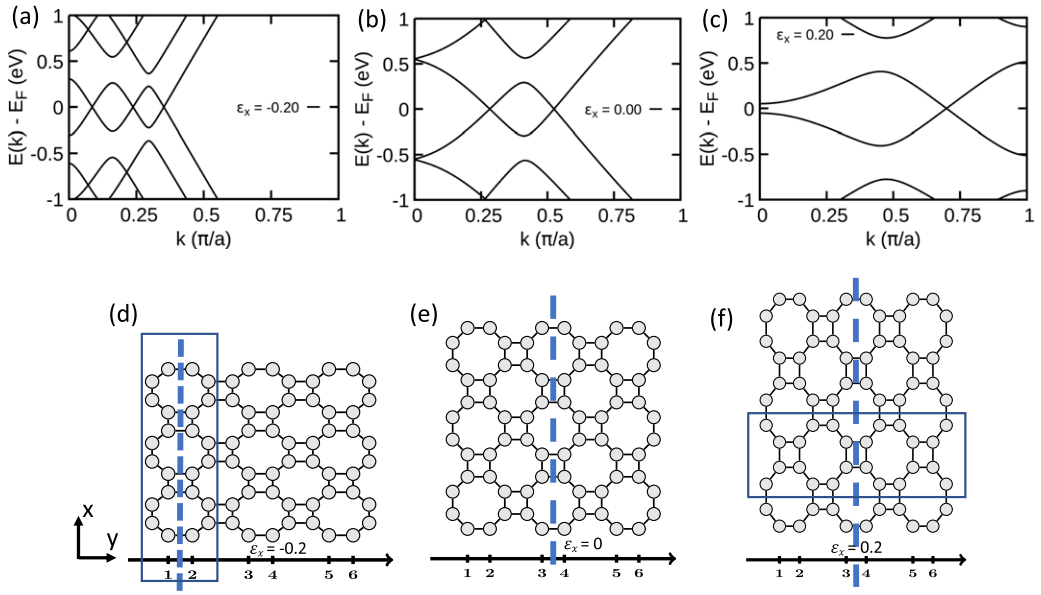

Figure 5. Band structures for the 6-ATGNR with (a) −0.2, (b) zero and (c) 0.2 uniaxial strain (ϵ_x) applied along the ribbon length. Figures (d)–(f) show in relative scale, the structural modifications with multiple unit cells in the direction of periodicity (x-direction) used to highlight confinement and structural effects. In (d), compressive strain ϵ_x and shorter bond lengths lead to increased kinetics in the x-direction, resulting in an effective system of three, weakly-coupled 2-ATGNR chains and the three Dirac points in (a). The box highlights the direction of increased lateral confinement in y, and the dashed line indicates the structural symmetry of the effective 2-ATGNR. (e) shows the 6-ATGNR with zero strain having two structural symmetries, namely, the mirror symmetry indicated by the dashed line, and that of the symmetric tetrahedral sub-unit, which can be translated about this point resulting in the two Dirac points in (b) [23]. In (f), tensile strain in ϵ_x causes increased lateral confinement in y highlighted by the box. The loss of symmetry in the base tetrahedral-unit results in symmetry reduction with only the mirror symmetry remaining as indicated by the dashed line and single Dirac point in (c).

function of increasing ribbon width (figures 6(a)–(d)). Investigation of these points via band structure studies show that Dirac-point features occur at the band edge under extreme compressive strain only ($\epsilon_x = -0.164$ for the 3-ATGNR, $\epsilon_x = -0.180$ for the 5-ATGNR, $\epsilon_x = -0.187$ for the 7-ATGNR and $\epsilon_x = -0.192$ for the 9-ATGNR). Closer examination of the 5-ATGNR as an exemplar asymmetric system shows that in addition to the Dirac point and associated linear dispersion at the band-edge for $\epsilon_x = -0.180$, there is also a band-gap closure under tensile strain at $\epsilon_x = 0.067$, albeit with parabolic dispersion (figure 6(e)).

An explanation of the gap-closing features of the asymmetric 5-ATGNR can be found in the induced symmetry changes caused by strain effects, which are apparent in the structural modifications and TB features in table 2. In the case of the Dirac-point formation at high compressive strain ($\epsilon_x = -0.180$), the system approaches one of weakly-coupled, vertical chain units, such as the cleaved structure in figure 4(b) in reference [27], and similar also to the aforementioned, symmetric ATGNRs under compression, for example the 6-ATGNR in figure 5(d). In the case of the gap closing at positive, tensile strain ($\epsilon_x = 0.067$), the TB results (table 2) shows that all of the bond lengths become comparable in the 5-ATGNR, yielding a structural change towards a system with quasi-rectangular, structural symmetry. In both of these cases, the introduction of structural symmetries result in gap-closing mechanisms that overcome the native, structural asymmetry effects of the ATGNR.

Table 2. 5-ATGNR bond lengths and hopping parameters determined at the points where the band gap closes ($\epsilon_x = -0.180$ and 0.067) and at zero strain.

Strain	−0.180	0	0.067
Horiz. tetrabond (Å)	1.532	1.468	1.444
t_{ay} horizontal (eV)	[2.320]	[2.525]	[2.608]
Vert. tetrabond (Å)	1.203	1.468	1.567
t_{ax} vertical (eV)	[3.758]	[2.525]	[2.218]
Inter. tetrabond (diag.) (Å)	1.297	1.383	1.419
t_b diagonal (eV)	[3.223]	[2.835]	[2.693]

Dirac-point formation occurs for 2D-systems that map in the low-energy limit, to an effective two-band solution, having also an inherent, protective symmetry that allows for band crossing and degeneracy at high-symmetry k-points—the so-called von Neumann–Wigner theorem [30]. Against these criteria, graphene is classified as a class I Dirac system due to its inherent two-sublattice honeycomb structure that translates to a low-energy, two-band model having a degenerate solution and linear dispersion about the high-symmetry K and K' points. Underpinning this solution is the structural, three-fold rotational symmetry at each lattice point in graphene and reflection symmetry of its two sublattices [21], with robustness of the Dirac points to Brillouin-zone strain distortion being attributed to an underlying protective symmetry characterised by antiunitary operation [22]. In AGNRs, the Dirac points have been shown to be accessed via uniaxial strain that shifts these

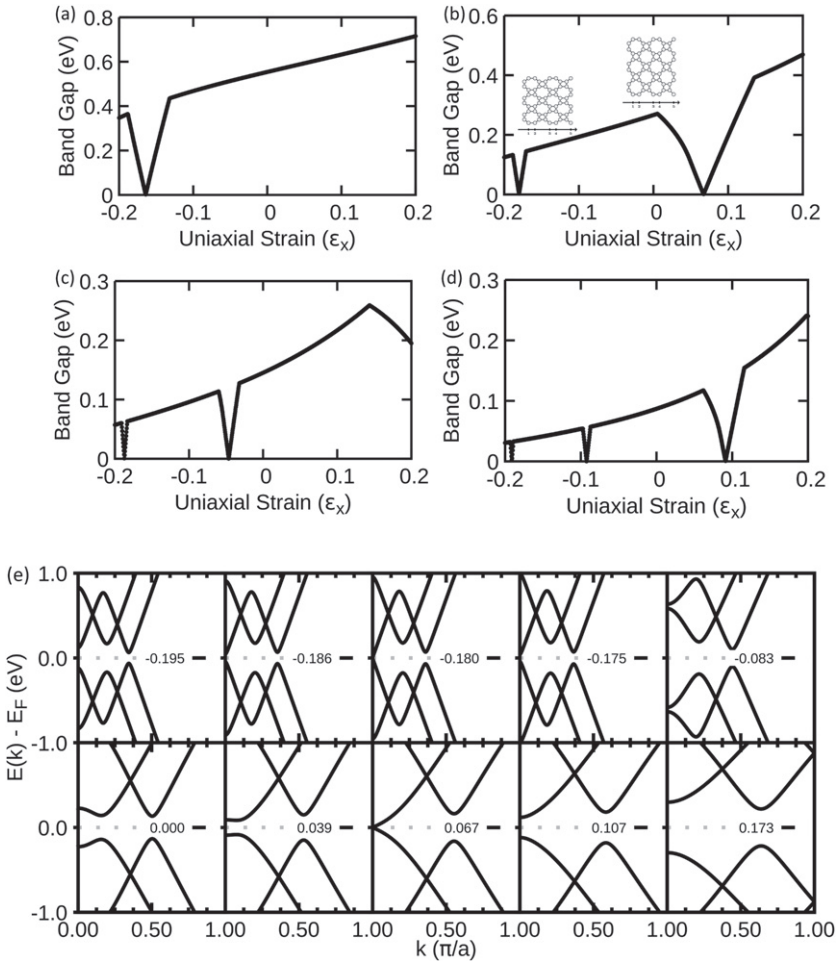

Figure 6. Band gap as a function of uniaxial strain (ϵ_x) applied along the ribbon length for the (a) 3-ATGNR, (b) 5-ATGNR, (c) 7-ATGNR, (d) 9-ATGNR systems. To capture the narrow closing of the band-gaps in (a)–(d), 0.0001-increment calculations in ϵ_x were applied over the full strain range, with this degree of computation being tractable via tight binding. (e) Corresponding band structures as a function of uniaxial strain (ϵ_x) for the 5-ATGNR.

points in *k*-space so that they coincide with the allowed discrete AGNR *k*-values [31].

In comparison, the ATGNRs studied in this work are classified as class II Dirac systems, whereby Dirac-point formation results from the inherent mirror-symmetry in the real-space structure [21, 23]. Such effects are most apparent in unstrained mirror-symmetric ATGNRs, which have Dirac points versus asymmetric gapless ATGNRs. For ATGNRs with uniaxial strain, we have demonstrated the preservation of the Dirac points and the number of these to be related to changes in symmetry and quantum confinement effects due to real-space structural modifications. Preservation of the structural mirror-symmetry is critical for preserving the single Dirac-point feature of these systems as per the von Neumann–Wigner theorem, and is shown, for example, by the 6-ATGNR under tensile strain (figure 5(c)). Introduction of structural symmetry, as in the 5-ATGNR with tensile strain (figure 6(b)), can also fulfil the essential symmetry requirement where mirror symmetry is not intrinsic, in this case by the mapping of this system to a quasi-rectangular structure, which has also been shown to be a class II Dirac system [21].

4. Conclusion

Application of uniaxial strain in symmetric and asymmetric ATGNRs has been studied using a nearest-neighbour, TB model. Symmetry-based arguments are used to explain the displacement of the Dirac point in *k*-space and gap-closing mechanisms in these systems caused by structural perturbations upon application of uniaxial strain. The linear dispersion and associated Dirac points are shown to be robust against structural modification in symmetric ATGNRs, with capability demonstrated for multi Dirac-point formation for systems under compressive uniaxial strain. For asymmetric ATGNRs, symmetry-inducing structural changes under compressive strain result in gap-closing mechanisms, including Dirac-point formation, that overcome limitations due to structural asymmetry. We hope these investigations add fundamental understanding to the role of symmetry in the formation of relativistic properties (Dirac features) and stimulate future DFT studies, as well as greater research, in general, into ATGNRs, which show potential for strain engineering of relativistic properties within the realm of flexible electronics.

Data availability statement

The data that support the findings of this study are available upon reasonable request from the authors.

Acknowledgement

YH would like to thank the guest editors for the invitation to submit to this special issue of Women in Computational Condensed Matter Physics.

ORCID iDs

Y Hancock https://orcid.org/0000-0003-4799-2783

References

[1] Novoselov K S, Fal'ko V I, Colombo L, Gellert P R, , Schwab M G and Kim K 2012 *Nature* **490** 192
[2] Semenoff G W 1984 *Phys. Rev. Lett.* **53** 2449
[3] Katsnelson M I 2007 *Mater. Today* **10** 20
[4] Han M Y, Özyilmaz B, Zhang Y and Kim P 2007 *Phys. Rev. Lett.* **98** 206805
[5] Son Y-W, Cohen M L and Louie S G 2006 *Phys. Rev. Lett.* **97** 216803
[6] Kang J, He Y, Zhang J, Yu X, Guan X and Yu Z 2010 *Appl. Phys. Lett.* **96** 252105
[7] Vogt P, De Padova P, Quaresima C, Avila J, Frantzeskakis E, Asensio M C, Resta A, Ealet B and Le Lay G 2012 *Phys. Rev. Lett.* **108** 155501
[8] Ge M *et al* 2021 *Mater. Today Nano* **15** 100119
[9] Munkhbat B, Yankovich A B, Baranov D G, Verre R, Olsson E and Shegai T O 2020 *Nat. Commun.* **11** 4604
[10] Tomańek D 2020 *Phys. Rev. Appl.* **13** 030001
[11] Wang J, Deng S, Liu Z and Liu Z 2015 *Natl Sci. Rev.* **2** 22
[12] Novoselov K S, Geim A K, Morozov S V, Jiang D, Katsnelson M I, Grigorieva I V, Dubonos S V and Firsov A A 2005 *Nature* **438** 197
[13] Bao W, Liu G, Zhao Z, Zhang H, Yan D, Deshpande A, LeRoy B and Lau C N 2010 *Nano Res.* **3** 98
[14] Choi S-M, Jhi S-H and Son Y-W 2010 *Phys. Rev.* B **81** 081407
[15] Jia T-T, Zheng M-M, Fan X-Y, Su Y, Li S-J, Liu H-Y, Chen G and Kawazoe Y 2016 *Sci. Rep.* **6** 18869
[16] Sugita Y, Miyake T and Motome Y 2018 *Phys. Rev.* B **97** 035125
[17] Liu Y, Wang G, Huang Q, Guo L and Chen X 2012 *Phys. Rev. Lett.* **108** 225505
[18] Bandyopadhyay A, Datta S, Jana D, Nath S and Uddin M M 2020 *Sci. Rep.* **10** 2502
[19] Malko D, Neiss C, Viñes F and Görling A 2012 *Phys. Rev. Lett.* **108** 086804
[20] Majidi R 2017 *Theor. Chem. Acc.* **136** 109
[21] van Miert G and Smith C M 2016 *Phys. Rev.* B **93** 035401
[22] Hou J-M and Chen W 2015 *Sci. Rep.* **5** 17571
[23] Dai C J, Yan X H, Xiao Y and Guo Y D 2014 *Europhys. Lett.* **107** 37004
[24] Hancock Y, Uppstu A, Saloriutta K, Harju A and Puska M J 2010 *Phys. Rev.* B **81** 245402
[25] Harrison W A 1980 *Electronic Structure and the Properties of Solids: The Physics of the Chemical Bond* (San Francisco, CA: Freeman)
[26] White C T, Li J, Gunlycke D and Mintmire J W 2007 *Nano Lett.* **7** 825
[27] Fthenakis Z G and Lathiotakis N N 2015 *Phys. Chem. Chem. Phys.* **17** 16418
[28] Sun H, Mukherjee S, Daly M, Krishnan A, Karigerasi M H and Singh C V 2016 *Carbon* **110** 443
[29] Sui C, Zhao Y, Zhang Z, He J, Zhang Z, He X, Wang C and and Wu J 2017 *ACS Omega* **2** 3977
[30] von Neumann J and Wigner E 1929 *Phys. Z.* **30** 467
Hettema H (ed) 2000 Quantum Chemistry, Classic Scientific Papers (*Word Scientific Series in 20th Century Chemistry* vol 8) (Singapore: World Scientific) pp 25–31 (Engl. transl.)
[31] Li Y, Jiang X, Liu Z and Liu Z 2010 *Nano Res.* **3** 545